

Search for a spin–nematic phase in the quasi-one-dimensional frustrated magnet LiCuVO_4

N. Büttgen,^{1,*} K. Nawa,^{2,3} T. Fujita,⁴ M. Hagiwara,⁴ P. Kuhns,⁵ A. Prokofiev,⁶ A.P. Reyes,⁵ L.E. Svistov,^{7,†} K. Yoshimura,² and M. Takigawa^{3,‡}

¹*Center for Electronic Correlations and Magnetism (EKM),*

Experimentalphysik V, Universität Augsburg, D-86135 Augsburg, Germany

²*Department of Chemistry, Graduate School of Science, Kyoto University, Kyoto 606-8502, Japan*

³*Institute for Solid State Physics, The University of Tokyo, Kashiwanoha, Kashiwa, Chiba, 277-8581, Japan*

⁴*Center for Advanced High Magnetic Field Science, Graduate School of Science,*

Osaka University, Machikaneyama 1-1, Toyonaka, Osaka 560-0043, Japan

⁵*National High Magnetic Field Laboratory, Tallahassee, Florida 32310, USA*

⁶*Institut für Festkörperphysik Technische Universität Wien, A-1040 Wien, Austria*

⁷*P.L. Kapitza Institute for Physical Problems RAS, 119334 Moscow, Russia*

(Dated: May 2, 2018)

We have performed NMR experiments on the quasi one-dimensional frustrated spin-1/2 system LiCuVO_4 in magnetic fields H applied along the c -axis up to field values near the saturation field H_{sat} . For the field range $H_{c2} < H < H_{c3}$ ($\mu_0 H_{c2} \approx 7.5$ T and $\mu_0 H_{c3} = [40.5 \pm 0.2]$ T) the ^{51}V NMR spectra at $T = 380$ mK exhibit a characteristic double-horn pattern, as expected for a spin-modulated phase in which the magnetic moments of Cu^{2+} ions are aligned parallel to the applied field H and their magnitudes change sinusoidally along the magnetic chains. For higher fields, the ^{51}V NMR spectral shape changes from the double-horn pattern into a single Lorentzian line. For this Lorentzian line, the internal field at the ^{51}V nuclei stays constant for $\mu_0 H > 41.4$ T, indicating that the majority of magnetic moments in LiCuVO_4 are already saturated in this field range. This result is inconsistent with the previously observed linear field dependence of the magnetization $M(H)$ for $H_{c3} < H < H_{\text{sat}}$ with $\mu_0 H_{\text{sat}} = 45$ T [L. E. Svistov *et al.*, JETP Letters **93**, 21 (2011)]. We argue that the discrepancy is due to non-magnetic defects in the samples. The results of the spin-lattice relaxation rate of ^7Li nuclei indicate an energy gap which grows with field twice as fast as the Zeeman energy of a single spin, therefore, suggesting that the two-magnon bound state is the lowest energy excitation. The energy gap tends to close at $\mu_0 H \approx 41$ T. Our results suggest that the theoretically predicted spin–nematic phase, if it exists in LiCuVO_4 , can be established only within the narrow field range $40.5 < \mu_0 H < 41.4$ T.

PACS numbers: 75.50.Ee, 76.60.-k, 75.10.Jm, 75.10.Pq

I. INTRODUCTION

The search for novel quantum states in strongly correlated electronic systems exhibiting an exotic order is at the core of modern condensed matter physics. An example that attracts strong recent interest is the *nematic phase*. Analogous to the nematic state observed in liquid crystals, electronic correlation in a nematic phase develops a *preferred orientation*, which breaks rotational symmetry. However, time reversal symmetry is preserved unlike in a conventional magnetic order. The possibility of such nematic order has been discussed in several different systems such as frustrated magnets,^{1,2} iron–pnictide superconductors,³ and heavy–fermion materials.⁴

Among them, one-dimensional (1D) frustrated quantum spin systems ($S = 1/2$) having a ferromagnetic nearest neighbor (NN) exchange interaction J_1 and an antiferromagnetic next-nearest neighbor (NNN) interaction J_2 ,

$$\mathcal{H} = J_1 \sum_n \mathbf{S}_n \cdot \mathbf{S}_{n+1} + J_2 \sum_n \mathbf{S}_n \cdot \mathbf{S}_{n+2} \quad (1)$$

in magnetic fields deserve particular attention since extensive theoretical efforts have been devoted to this

model.^{5–17} Such intrachain interactions together with ferromagnetic interchain coupling in the case of large spin values yield a rich magnetic phase diagram.¹⁸ In particular, the case $|J_1/(4J_2)| < 1$ leads to a helical magnetically ordered structure. In principle, a true long-range magnetically ordered structure of a 1D chain of magnetic moments is suppressed by spin fluctuations, and a magnetic state of such a system is characterized by short-range correlations between the magnetic moments. But according to theory, a long-range magnetic order can be stabilized due to interactions beyond Eq. (1), i.e., interactions with an applied magnetic field, interactions with the crystalline environment, or interactions between magnetic chains. For instance a moderate static magnetic field H stabilizes helical correlations in favour of a long-range ordered state even in one dimension^{7,8} with the order parameter $\langle \mathbf{S}_n \times \mathbf{S}_{n+1} \rangle_z = \langle S_n^x S_{n+1}^y - S_n^y S_{n+1}^x \rangle$ for $S = 1/2$ and $H \parallel z$. In contrast to the helical magnetic structure the expectation values of the transverse spin components $\langle S_n^x \rangle$ and $\langle S_n^y \rangle$ are equal to zero. Such magnetic state with this pseudovector order parameter was labeled the chiral phase in the literature. To our knowledge, this chiral phase has not been observed experimentally.

One-dimensional frustrated quantum spin systems with competing exchange interactions given by Eq. (1) are intriguing also in high magnetic fields, near the saturation field H_{sat} . Let us first consider the fully polarized ground state above the saturation field $H > H_{\text{sat}}$. In ordinary unfrustrated antiferromagnets, the lowest energy excitation is described by a single spin-flip, or a magnon, which acquires kinetic energy due to exchange interactions, forming a dispersive magnon band. As the field is reduced, the excitation gap determined by the minimum energy of the magnon band vanishes at H_{sat} . Below H_{sat} , the Bose-Einstein condensation (BEC) of magnons occurs in the presence of finite three-dimensional interchain coupling, resulting in an antiferromagnetic order in the plane perpendicular to the field with the order parameter $(-1)^n < S_n^- + H.c. >$ (Ref. 19,20).

In contrast, the lowest energy excitation in the frustrated chain of Eq. (1) immediately above H_{sat} is a bound magnon pair, not a single spin-flip, stabilized by the ferromagnetic NN interaction for a wide range of the ratio J_1/J_2 (Refs. 5–9,21–23). Below H_{sat} , these bound magnon pairs exhibit BEC in the presence of special-type interchain coupling and establish a long-range ordered magnetic structure with the order parameter given by $(-1)^n < S_n^- S_{n+1}^- + H.c. > = (-1)^n < (S_n^x S_{n+1}^x - S_n^y S_{n+1}^y) >$ (Refs. 12–17). This type of magnetic order in the recent literature is labeled as *nematic*. Again, the nematic order breaks the spin rotational symmetry. More precisely, the preferred orientation of the nearest neighbor spin correlation (director) rotates 90° from one bond to the next. However, the transverse components $\langle S_n^x \rangle$ and $\langle S_n^y \rangle$ are zero and the longitudinal magnetization remains uniform, $\langle S_n^z \rangle = M/N$, where M is the bulk magnetization and N is the number of magnetic ions of the sample.

As the field is further decreased, theories predict that the nematic order is replaced by a spin-density-wave (SDW) state, where the moments are collinear with the external field and their magnitudes are modulated with a generally incommensurate periodicity.^{7–9,14–16} This SDW state can be regarded as a spatial order of the bound magnon pairs stabilized by their mutual repulsive interaction, which becomes dominant over the gain in the kinetic energy of the BEC phase as the density of bound magnon pairs increases.

A promising candidate compound where these theoretical predictions are expected to be tested experimentally is the antiferromagnet LiCuVO_4 , which contains frustrated chains of Cu^{2+} ($S = 1/2$) along the crystallographic b -direction.²⁴ Let us first summarize the results of the previous studies on the magnetic phases of LiCuVO_4 for fields lower than $\mu_0 H = 30$ T (Refs. 25–33). At zero field, an incommensurate planar spiral structure is realized below $T_N \approx 2.3$ K with the moments lying in the ab -plane.^{25,26} A spin-flip transition occurs at $\mu_0 H_{c1} = 2.5$ T, flipping the moments into the plane perpendicular to the field.²⁸ In higher fields $H > H_{c2}$ ($\mu_0 H_{c2} \approx 7.5$ T) a collinear spin-modulated

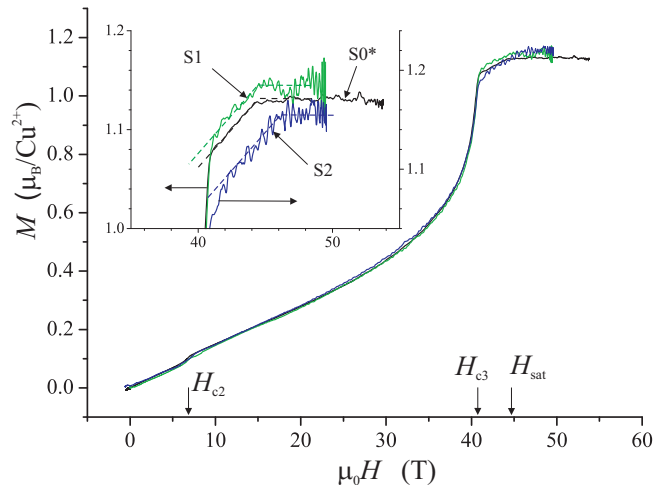


FIG. 1: Magnetization $M(H)$ measured in pulsed magnetic fields H oriented $\mathbf{H} \parallel \mathbf{c}$ at $T = 1.3$ K in LiCuVO_4 . Inset: Magnification of $M(H)$ for fields around the saturation field H_{sat} . Data of three different single crystals S1, S2 and S0* are shown, where the data of S0* are taken from Ref. 34. The dashed lines are parallel to each other and guide the eye. The $M(H)$ data for the samples S1 and S2 are more noisy than for S0*, because these samples are significantly smaller.

structure is realized,^{28–31,33} consistent with the theoretical prediction.^{7–9,14–16} Remarkably, the relation between the magnetization and the wave vector of the spin-modulated structure measured by neutron diffraction experiments in fields up to 15 T demonstrates that it is the bound magnon pairs with $S_z = 2$ that form a periodic structure.^{32,33} Also the temperature dependence of the nuclear spin-lattice relaxation rate $1/T_1$ at the V sites indicates the development of an energy gap in the transverse spin excitation spectrum above T_N ,³¹ which corresponds to the binding energy of magnon pairs, as theoretically predicted.^{10,11} The observation of the spin-modulated phase and the experimental proof for the bound magnon pairs provide strong support that LiCuVO_4 is indeed well described by the model of Eq. (1).

By further increase of the applied magnetic field H , it is expected that the spin-nematic phase develops before the magnetization saturates at H_{sat} . In recent experiments the field dependent magnetization curve $M(H)$ of LiCuVO_4 exhibited anomalies slightly below $\mu_0 H_{\text{sat}} \approx 45$ T, indicating a new phase.³⁴ Figure 1 shows $M(H)$ for three different samples measured in pulsed magnetic fields H applied along the c -direction at $T = 1.3$ K. In addition to the anomalies at H_{c2} and H_{sat} already mentioned, all samples show another anomaly at $\mu_0 H_{c3} \approx 40.5$ T, about 5 T below the saturation. The sharp increase of the magnetization towards higher field stops at $\mu_0 H_{c3}$. The magnetization then increases linearly in the field range $H_{c3} \lesssim H < H_{\text{sat}}$ with the slope $\approx 1/2 \cdot M_{\text{sat}}/H_{\text{sat}}$. This magnetization behavior near saturation including the slope of $M(H)$ for $H_{c3} \lesssim H < H_{\text{sat}}$ is very similar for all sample.

In this paper we discuss the NMR spectra of ^{51}V nuclei and the nuclear spin–lattice relaxation rate $1/T_1$ of ^7Li nuclei for applied magnetic fields H along the c -direction ($\mathbf{H} \parallel \mathbf{c}$) near the saturation field $\mu_0 H_{\text{sat}} \approx 45$ T. The NMR spectra represent distributions of the internal magnetic fields which are produced by the surrounding magnetic Cu^{2+} moments. The internal field has a large distribution in the spin–modulated phase leading to broad NMR spectra. In the nematic phase, in contrast, moments are uniform and we expect a sharp single, solitary NMR line similar to the saturated phase. However, unlike in the saturated phase, the internal field determined from the peak position of the spectrum should change with the magnetic field H as it is the case for the bulk magnetization $M(H)$ in the nematic phase. Such expectation may not be realized if the sample contains defects, which generate inhomogeneous distribution of the magnetic moments. Since the NMR spectra reflect the histogram of magnetic moments while $M(H)$ gives average magnetization, they may behave differently as we discuss below.

II. EXPERIMENTAL RESULTS

The observation of the phase transition from the spin–modulated phase to the magnetically saturated phase from a local point of view is the major subject of the present work. In addition to $M(H)$ measurements, which give bulk properties, we employed NMR of ^{51}V ($I = 7/2$, $\gamma = 2\pi \times 11.1988$ MHz/T) nuclei probing the local magnetic properties of the Cu^{2+} moments in LiCuVO_4 . Three single–crystalline samples were used in the NMR measurements: sample S0, S1, and S2. Sample S0 was used in the previous NMR experiments in Refs. 28–30 and obtained from the same batch as S0* whose $M(H)$ curve is shown in Fig. 1. Samples S1 and S2 are from a new batch whose $M(H)$ curves are also shown in Fig. 1. Spin–echo techniques were utilized in the hybrid 45 T magnet of the DC field facility at the National High Magnetic Field Laboratory (NHMFL), Tallahassee, Florida. The absolute values of the applied magnetic fields H were calibrated by NMR using aluminum powder. All spectra of sample S0 were collected with the pulse sequence $3\mu\text{s} - \tau - 3\mu\text{s}$ ($\tau = 15\mu\text{s}$) by sweeping the applied magnetic field H at constant frequencies. Spectra of the single–crystalline samples S1 and S2 were recorded by summing the Fourier transform of the spin–echo signal with the pulse sequence $2.5\mu\text{s} - \tau - 2\mu\text{s}$ ($\tau = 17\mu\text{s}$) obtained for equally spaced excitation frequencies at a fixed magnetic field. Temperatures down to $T = 380$ mK were achieved within a ^3He cryostat.

Figure 2 shows the NMR spectra of sample S2 obtained at $T = 380$ mK within the range $38 \leq \mu_0 H \leq 45$ T of the applied magnetic field H for $\mathbf{H} \parallel \mathbf{c}$. Note that $\nu/\gamma \equiv \mu_0 H_{\text{eff}}$ represents the effective magnetic field sensed by nuclei being observed at the resonance frequency ν and is the sum of the applied field plus the inter-

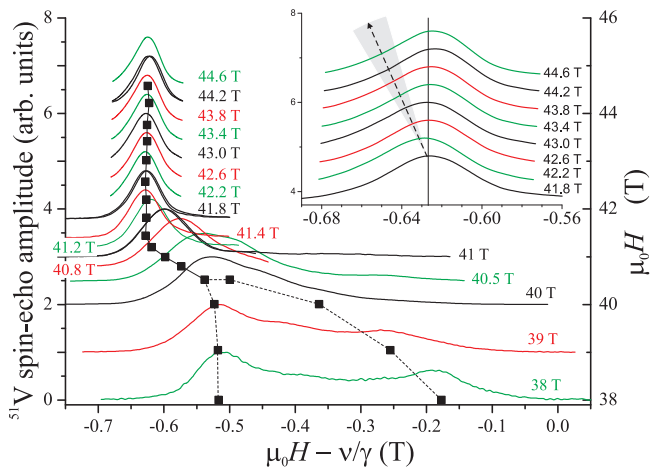


FIG. 2: ^{51}V NMR spectra obtained from crystal S2 at $T = 380$ mK within the field range $38 \leq \mu_0 H \leq 45$ T for $\mathbf{H} \parallel \mathbf{c}$. The spin-echo amplitudes are normalized by the peak intensity. The spectral shape shows a crossover at $\mu_0 H_{c3} \approx 40.5$ T from the double-horn pattern at lower fields to the single-peak pattern at higher fields. The dashed arrow in the inset denotes the expected line shift which is estimated from the bulk magnetization $M(H)$.

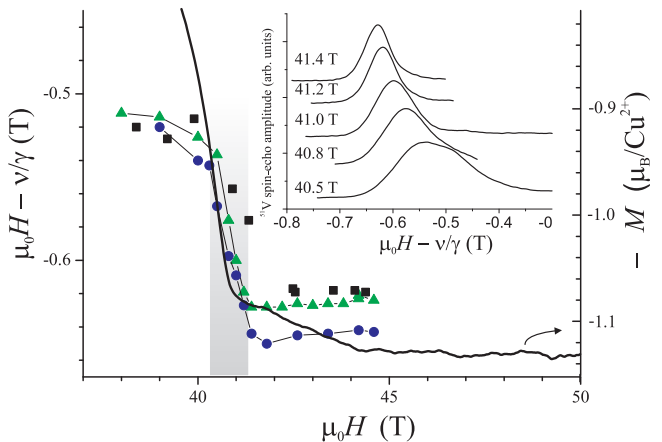


FIG. 3: Peak positions of the ^{51}V NMR spectra in LiCuVO_4 are plotted against applied field along the c -direction obtained from samples S0 (squares), S1 (triangles), and S2 (bullets), respectively (left axis). The solid line shows the bulk magnetization $M(H)$ vs. the applied magnetic field H obtained from sample S0* (right axis). Inset: ^{51}V NMR spectra of sample S2.

nal local field due to Cu^{2+} moments, i.e., $H_{\text{eff}} = H + H_{\text{int}}$. Therefore, the abscissa axis of the spectra in Fig. 2 $\mu_0 H - \nu/\gamma$ is equal to $-\mu_0 H_{\text{int}}$ at the probing ^{51}V nuclei. The double-horn shaped pattern for lower fields H at the bottom of Fig. 2 resemble our previous results,^{28–30} where we established the spin–modulated magnetic structure in LiCuVO_4 . The asymmetry of the double-horn shaped pattern for $\mu_0 H < 30$ T turned out to be due to different spin–spin relaxation times T_2 at different spectral positions.³⁰ Around the value of the applied magnetic

field $\mu_0 H_{c3} = 40.5$ T the double-horn shape starts to disappear in favor of a single-peak spectrum evolving a more symmetric line shape towards higher magnetic fields H .

For applied magnetic fields H higher than $\mu_0 H > 41.4$ T, the internal field occurs to stay almost constant without any shift in the peak position of the spectral line. This observation is in contrast to the $M(H)$ data which further increase linearly for the same field values up to the saturation field H_{sat} (cf. the inset in Fig. 1). This conflict is illustrated in the inset of Fig. 2, where the almost unshifted NMR spectral lines are plotted together with the internal field fields calculated from the $M(H)$ data (dashed arrow). The shaded sector in the inset of Fig. 2 shows the estimated error made for the slope of the $M(H)$ dependence obtained from pulse field experiments on $M(H)$ (cf. Fig. 1). Such unexpected behavior was observed for all three studied samples. The field dependences of the peak positions of the ^{51}V NMR spectra are shown in Fig. 3 together with the $-M(H)$ data. The internal field at the vanadium nuclei for all three samples shows almost no change with field for $\mu_0 H > 41.4$ T in contrast to the full magnetic moment of the sample $M(H)$ measured in the same field range. This discrepancy between NMR line shift and bulk magnetization $M(H)$ demonstrates that the magnetization is not uniform, probably due to the presence of defects. The constant internal field at the peak of the intense NMR line indicates that the majority part of the nuclei far from defects is embedded in an electronic surrounding with saturated magnetic moments, while the bulk magnetization is affected by defects. This point is discussed in more detail below. Therefore, the NMR result is seemingly ineffective in detecting the existence of a spin nematic phase expected within the field range $H_{c3} < H < H_{\text{sat}}$ previously.

However, close inspection of the data in Fig. 3 reveals that within a limited narrow field range $40.5 \leq \mu_0 H \leq 41.4$ T (indicated by the shaded area in Fig. 3) the NMR spectral pattern is characterized by a nearly symmetric, solitary, single peak whose resonance position shifts strongly depending on the applied magnetic field H (cf. the inset of Fig. 3). This observation meets the theoretically predicted behavior of the spin-nematic phase. Indeed, the behavior of the NMR internal field within the restricted field range mentioned above is consistent with the theoretical prediction of a very steep slope of the magnetization curve in the nematic phase immediately below saturation.¹⁷

After the description of static magnetic properties probed by ^{51}V NMR mentioned above, we now turn to dynamic properties and the results of the nuclear spin-lattice relaxation rate $1/T_1$ of ^7Li nuclei ($I=3/2$, $\gamma = 2\pi \times 16.5466$ MHz/T). The sample used for the $1/T_1$ measurements is none of the three samples used for the ^{51}V NMR, but is from the same batch as the sample used in one of the previous NMR experiments described in Ref. 31. Figure 4 shows the temperature dependence

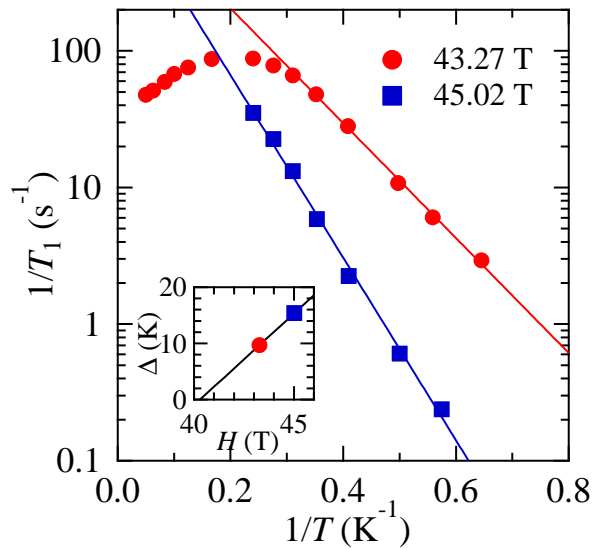


FIG. 4: Temperature dependence of the spin-lattice relaxation rate $1/T_1$ at ^7Li nuclei in Arrhenius representation measured for different applied magnetic fields $\mu_0 H = 43.27$ T and 45.02 T. Inset: The slopes of the Arrhenius representations, i.e. activation energies Δ , plotted vs. the applied magnetic field H . The solid line indicates a linear fit (see text).

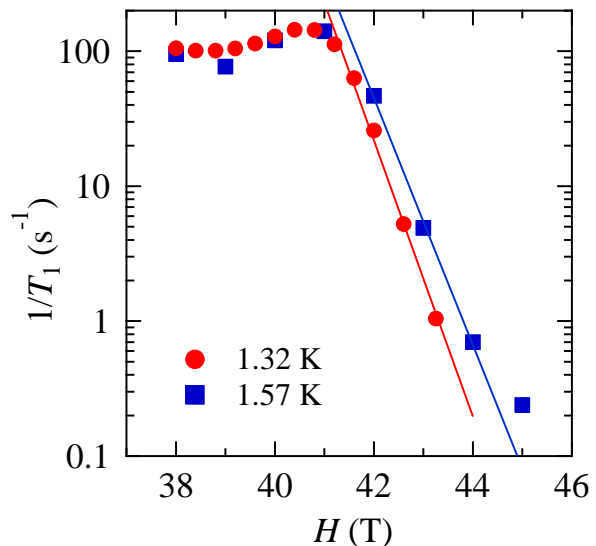


FIG. 5: Field dependence of the spin-lattice relaxation rate $1/T_1$ at ^7Li nuclei for different temperatures.

of $1/T_1$ at two different applied magnetic fields above $\mu_0 H = 41.4$ T. The Arrhenius representation of the data exhibits a thermally activated behavior at low temperatures

$$\frac{1}{T_1} \propto \exp\left(-\frac{\Delta}{T}\right). \quad (2)$$

The activation energies are obtained as $\Delta = 15.4$ K at

45.02 T and $\Delta = 9.7$ K at 43.27 T (see the inset of Fig. 4). Assuming that the activation gap depends linearly on the field H ,

$$\Delta = D(H - H_0), \quad (3)$$

we obtain $D = 3.3$ K/T. In ordinary antiferromagnets, where the lowest energy excitations in the saturated state are single spin-flip processes involving the change of magnetization by $\Delta S_z = 1$, the excitation gap should be given by $g_c \mu_B (H - H_{\text{sat}})$ with $g_c \mu_B = 1.55$ K/T ($g_c = 2.31$, Ref. 35). Remarkably, the value of D is much larger than $g_c \mu_B$ but close to $2g_c \mu_B = 3.1$ K/T. This indicates that the lowest-energy excitations are bound magnon pairs with $\Delta S_z = 2$.

The assumption of the linear field dependence of the energy gap is indeed justified by the exponential field dependence of $1/T_1$ above 41 T

$$\frac{1}{T_1} \propto \exp(-AH) \quad (4)$$

as shown in figure 5. From the plots for two different temperature values we obtain $A = 2.34$ T⁻¹ for $T = 1.32$ K and $A = 2.10$ T⁻¹ for $T = 1.57$ K. By relating Eq. (4) to Eqs. (2) and (3), we obtain $D = 3.1$ K/T (3.2 K/T) for $T = 1.32$ K ($T = 1.57$ K). These values are again close to $2g_c \mu_B$, consistent with the picture that the lowest excitation is a two-magnon bound state.

From the plot in the inset of Fig. 4, we expect the excitation gap to become zero at applied magnetic fields $\mu_0 H \approx 41$ T. This value is different from $\mu_0 H_{\text{sat}} = 45$ T determined from the magnetization data but agrees with the field value above which the ⁵¹V NMR spectral peak stays constant. This fact provides further support for our previous conclusion that a majority of the magnetic copper ions in LiCuVO₄ are already saturated *below* $\mu_0 H_{\text{sat}} = 45$ T.

III. DISCUSSION

We first discuss the ⁵¹V NMR spectra in the field range $H_{c2} < H < H_{c3}$, where the magnetically ordered structure is recognized as the spin-modulated structure. The characteristic double-horn shape (cf. Fig. 2) is an unambiguous fingerprint of an incommensurate magnetic structure only observed within this field range. For lower applied magnetic fields $H < H_{c2}$ or higher fields $H > H_{c3}$ the ⁵¹V NMR spectra consist of a single peak. The field dependence of the internal fields at the spectral maxima of the low-field and high-field horn in the case of the double-horn pattern, as well as the internal field of the singly peaked spectra are plotted in Fig. 6 (left axis). The arithmetically averaged field values H_{max} (solid bullets) of the high-field (triangles) and low-field (squares) maxima, together with the single-peak maxima tightly follow the field dependence of the magnetization data $M(H)$ (right axis in Fig. 6).

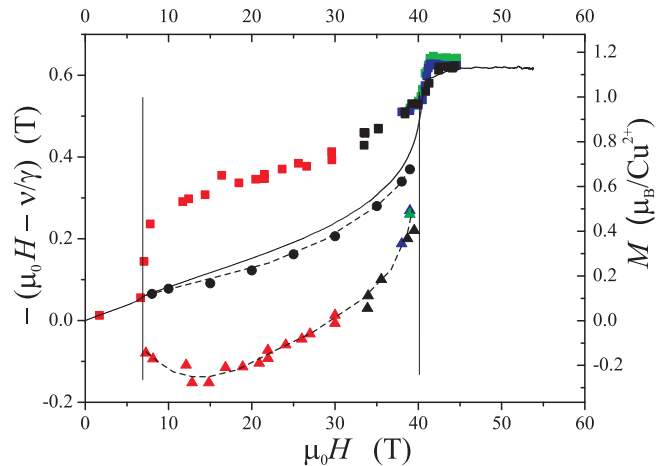


FIG. 6: Left axis: Field dependence of the ⁵¹V spin-echo maxima of the double-horn pattern shown in Fig. 2 (red symbols are data taken from Ref. 30). The other symbols denote the data of samples S0 (black), S1 (blue), and S2 (green), respectively. The bullets denote the arithmetic average of high-field (triangles) and low-field (squares) maxima. The dashed lines guide the eye. Right axis: The black solid line is the magnetization measurement $M(H)$ of sample S0* taken from Ref. 34.

We return to a closer inspection of the discrepancy between the internal field at the majority of vanadium nuclei obtained from NMR experiments and the bulk magnetization $M(H)$ observed within the range of applied magnetic fields $H_{c3} < H < H_{\text{sat}}$. The natural explanation for this phenomenon is the non-uniform magnetization of the sample, i.e., the magnetization of the majority part of the sample is saturated already at $\mu_0 H = 41.4$ T, whereas there are local regions within the sample whose magnetization is saturated only at H_{sat} . In such a case, the intense line of the NMR spectra in the high-field range is ascribed to the nuclei surrounded by magnetic moments with the saturated magnetization, whereas the experimentally observed growth of the bulk magnetization $M(H)$ of all the samples can be attributed to the non-saturated region near defects.

The expected magnetic structures for the field ranges $H_{c2} < H < H_{c3}$, $H_{c3} < H < H_{\text{sat}}$, and $H > H_{\text{sat}}$ are illustrated in Figs. 7 A, C, and D, respectively. The structures in panel A (below H_{c3}) and C (above H_{c3}) both exhibit longitudinal modulation of the magnetization. In case of the spin-modulated phase (A) this modulation has a regular sinusoidal shape, whereas for the high-field phase (C) the modulation is not periodic but accidental. We expect that the latter structure is associated with crystallographic defects. Although the nature of the defects is not precisely known, a composition study of LiCuVO₄ indicates the presence of Li defects of a few percents even in carefully prepared crystals.²⁴ It was argued that a Li deficiency produces a hole doped into the oxygen sites, which in turn will form a Zhang-Rice singlet with a Cu spin.^{24,36} Such a singlet should be

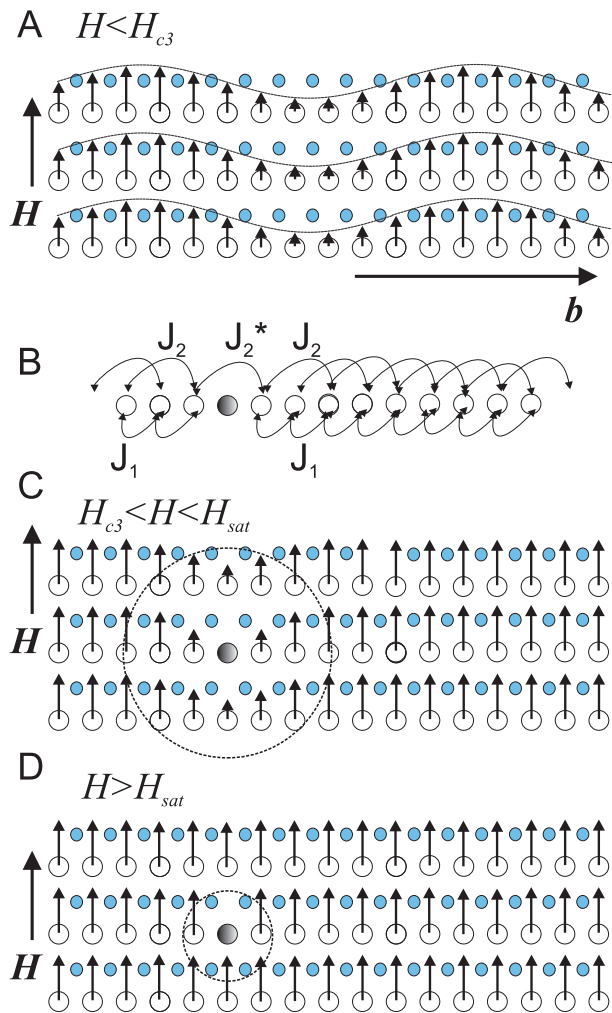


FIG. 7: Models of the magnetic structure projected along the a -axis for different field ranges, illustrating Cu^{2+} ions (large open circles), V^{5+} ions (small blue circles), and magnetic moments of Cu^{2+} (arrows). Panel A: the sinusoidal modulation below H_{c3} reconstructed from the values of μ_m and μ_1 obtained by fitting the ^{51}V NMR spectrum at $\mu_0 H = 38$ T, just below H_{c3} . Panel B: illustration of intrachain exchange bonds with a defect replacing a magnetic ion by a nonmagnetic one (gray bullet). Panels C and D: models of the magnetic structure with a defect for fields $H_{c3} < H < H_{\text{sat}}$ and $H > H_{\text{sat}}$, respectively. The dashed circles around the non-magnetic defect mark the region where the internal field of ^{51}V nuclei is smaller than the majority because the neighboring Cu moments are unsaturated.

equivalent to a non-magnetic defect replacing a Cu spin and provokes an unusual magnetic state in its vicinity with deleted two nearest ferromagnetic exchange bonds, but with a conserved antiferromagnetic bond between the two parts of the interrupted chain (see panel B of Fig. 7). A theoretical study shows that the saturation field of the magnetic neighborhood of such crystallographic defects is expected at distinctly higher fields compared to the saturation field of undisturbed magnetic chains.³⁷

In the following we describe the fingerprints of such

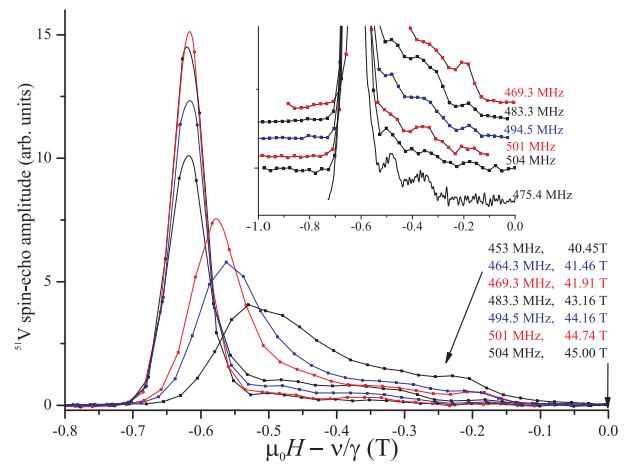


FIG. 8: ^{51}V NMR spectra of sample S0 obtained at $T = 380$ mK for different applied magnetic fields in the range $40.45 < \mu_0 H < 45$ T. Inset: Data for sample S2 are plotted additionally (solid line). The base lines of the different spectra in the inset are shifted along the y -axis for better visibility.

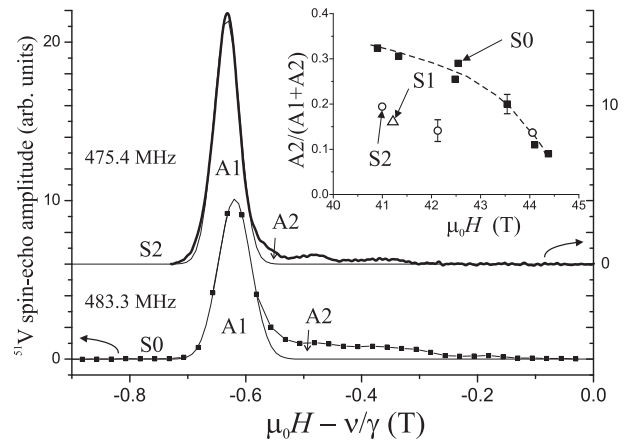


FIG. 9: ^{51}V NMR spectra at $T = 380$ mK for samples S0 and S2 measured at 483.3 and 475.4 MHz, respectively. Solid lines show the fitting results of the main peak of the spectral pattern with a Lorentzian line (A1). Inset: Relative integral intensity of the residual contribution A2 of the NMR spectra pattern which does not belong to the main line A1. Data from different samples S0 (solid squares), S1 (open triangle), and S2 (open circles) are shown.

defect structure found in our experiments and evaluate the concentration of those defects. Figure 8 is a replot of the field swept ^{51}V NMR spectra for applied magnetic fields H between $40.45 < \mu_0 H < 45$ T at 380 mK. Here, the ordinate axis is adjusted for each spectrum in such a way that the integrated intensity of the entire line is the same for all the spectra. This representation allows for an estimation of the defect concentration. The NMR spectra in this field range consist of an intense symmetric line and a broad plateau-like part. The latter component is closer to the diamagnetic reference field at $\mu_0 H - \nu/\gamma = 0$, and

hence has smaller internal fields. The intense symmetric line can be fit by a Lorentzian denoted A1 in Fig. 9, allowing us to separate the plateau-like part marked as A2. The inset of Fig. 9 shows the field dependence of the relative weight of the plateau-like part $A2/(A1+A2)$. For sample S0 this relative intensity of the plateau-like part decreases monotonously within the entire field range $H_{c3} < H < H_{sat}$, whereas for the samples S1 and S2 it was found to be smaller and to exhibit a weaker decrease with increasing field H .

The relative intensity $A2/(A1+A2)$ at fields in the vicinity of H_{sat} is approximately 0.1. From this value we can evaluate the defect concentration x : the probability p that all four magnetic sites surrounding the ^{51}V nucleus in its nearest proximity are occupied by Cu^{2+} ions is equal to $p = (1 - x)^4$. Here we suppose that defects are distributed randomly. On the other hand, this value can be evaluated as $A1/(A1 + A2) \approx 0.9$. From this equation we obtain the concentration $x = (2.5 \pm 0.6)\%$ of non-magnetic defects in reasonable agreement with the detailed investigation of reference 24.

IV. CONCLUSION

In conclusion, we investigated the magnetic structure of the Cu^{2+} moments in the quantum-spin chains of LiCuVO_4 in applied magnetic fields H up to the saturation field $\mu_0 H_{sat} = 45$ T. The double-horn shape of the ^{51}V NMR spectra in the incommensurate SDW phase changes to a single Lorentzian line around $\mu_0 H_{c3} = (40.5 \pm 0.2)$ T. Although the magnetization curve $M(H)$ shows a linear increase of magnetization in the field range $H_{c3} < H < H_{sat}$,³⁴ the internal field corresponding to the peak of the NMR spectra stays constant for $\mu_0 H > 41.4$ T, indicating that the moments surrounding the majority of vanadium nuclei are saturated in this field range.

The results of the nuclear spin-lattice relaxation rate of ^7Li nuclei also show an energy gap expected for bound magnon pairs above the saturation at $\mu_0 H \approx 41.4$ T. From these results, we conclude that the theoretically predicted nematic ordered phase can be realized only in the narrow field range $\mu_0 H_{c3} < \mu_0 H < 41.4$ T if it exists in LiCuVO_4 .

We have attributed the discrepancy between our NMR and magnetization data to effects caused by defects. From the careful investigation of a small pedestal-like contribution in the ^{51}V NMR spectra, we were able to quantify the number of magnetic defects. As these defects locally yield much higher saturation fields H_{sat} we reconciled our NMR results with recent magnetization $M(H)$ experiments.³⁴ Whether or not elimination of the defects stabilizes the spin-nematic phase is an interesting future issue.

Acknowledgments

This work is supported by the German Research Society (DFG) within the Transregional Collaborative Research Center TRR 80 (Augsburg, Munich), by the Grants 13-02-00637 of the Russian Foundation for Basic Research, Program of Russian Scientific Schools, by a Grant-in-Aid for Scientific Research 25287083 from the Japan Society of Promotion of Science, and by the Global CEO Program (Core Research and Engineering of Advanced Materials-Interdisciplinary Education Center for Materials Science)(No. G10) from MEXT, Japan. Work at the National High Magnetic Field Laboratory is supported by the NSF Cooperative Agreement No. DMR-0654118, and by the State of Florida. We thank H. Tsunetsugu, N. Shannon, A. Smerald, M. Sato, T. Momoi, T. Hikihara, H. T. Ueda, A. Matsuo, A. Smirnov, S. Sosin, O. Starykh, and M. Zhitomirsky for stimulating discussions.

* e-mail: norbert.buettgen@physik.uni-augsburg.de

† svistov@kapitza.ras.ru

‡ masashi@issp.u-tokyo.ac.jp

¹ A.F. Andreev and I.A. Grishchuk, *Sov. Phys. JETP* **60**, 267 (1984).

² K. Penc and A.M. Läuchli, *Introduction to Frustrated Magnetism*, edited by C. Lacroix, P. Mendels, and F. Mila (Springer, New York, 2011), p. 331.

³ S. Kasahara, H. J. Shi, K. Hashimoto, S. Tonegawa, Y. Mizukami, T. Shibauchi, K. Sugimoto, T. Fukuda, T. Terashima, A. H. Nevidomskyy and Y. Matsuda: *Nature* **486**, 382 (2012).

⁴ R. Okazaki, T. Shibauchi, H. J. Shi, Y. Haga, T. D. Matsuda, E. Yamamoto, Y. Onuki, H. Ikeda and Y. Matsuda: *Science* **331**, 439 (2011).

⁵ L. Kecke, T. Momoi, and A. Furusaki, *Phys. Rev. B* **76**, 060407(R) (2007).

⁶ T. Vekua, A. Honecker, H.-J. Mikeska, and F. Heidrich-Meisner, *Phys. Rev. B* **76**, 174420 (2007).

⁷ T. Hikihara, L. Kecke, T. Momoi, and A. Furusaki, *Phys. Rev. B* **78**, 144404 (2008).

⁸ J. Sudan, A. Lüscher, and A.M. Läuchli, *Phys. Rev. B* **80**, 140402(R) (2009).

⁹ F. Heidrich-Meisner, I.P. McCulloch, and A.K. Kolezhuk, *Phys. Rev. B* **80**, 144417 (2009).

¹⁰ M. Sato, T. Momoi, and A. Furusaki, *Phys. Rev. B* **79**, 060406(R) (2009).

¹¹ M. Sato, T. Hikihara, and T. Momoi, *Phys. Rev. B* **83**, 064405 (2011).

¹² M.E. Zhitomirsky and H. Tsunetsugu, *Europhys. Lett.* **92**, 37001 (2010).

¹³ S. Nishimoto, S.-L. Drechsler, R. Kuzian, J. Richter, J. Malek, M. Schmitt, J. van den Brink, and H. Rosner, *Europhys. Lett.* **98**, 37007 (2012).

¹⁴ H.T. Ueda and K. Totsuka, *Phys. Rev. B* **80**, 014417 (2009).

¹⁵ M. Sato, T. Hikihara, and T. Momoi, *Phys. Rev. Lett.* **110**, 077206 (2013).

- ¹⁶ O. A. Starykh and L. Balents, *Phys. Rev. B* **89**, 104407 (2014).
- ¹⁷ H. T. Ueda and K. Totsuka, arXiv: 1406.1960
- ¹⁸ T. Nagamiya, K. Nagata, and Y. Kitano, *Prog. Theor. Phys.* **27**, 1253 (1962).
- ¹⁹ T. Matsubara and H. Matsuda, *Prog. Theor. Phys.* **16**, 569 (1956).
- ²⁰ E. G. Batyev and L. S. Braginskii, *Sov. Phys. JETP* **60**, 781 (1984).
- ²¹ A.V. Chubukov, *Phys. Rev. B* **44**, 4693 (1991).
- ²² R. O. Kuzian and S.-L. Drechsler, *Phys. Rev. B* **75**, 024401 (2007).
- ²³ A. Smerald and N. Shannon, *Phys. Rev. B* **88**, 184430 (2013).
- ²⁴ A.V. Prokofiev, I.G. Vasilyeva, V.N. Ikorskii, V.V. Malakhov, I.P. Asanov, and W. Assmus, *J. Sol. State Chem.* **177**, 3131 (2004).
- ²⁵ B.J. Gibson, R.K. Kremer, A. V. Prokofiev, W. Assmus, and G.J. McIntyre, *Physica B* **350**, e253 (2004).
- ²⁶ M. Enderle, C. Mukherjee, B. Fåk, R.K. Kremer, J.-M. Broto, H. Rosner, S.-L. Drechsler, J. Richter, J. Malek, A. Prokofiev, W. Assmus, S. Pujol, J.-L. Raggazzoni, H. Rakoto, M. Rheinstädter, and H.M. Rønnow, *Europhys. Lett.* **70**, 237 (2005).
- ²⁷ C. Kogler, N. Büttgen, H.-A. Krug von Nidda, A. Loidl, R. Nath, A. V. Mahajan, A. V. Prokofiev, and W. Assmus, *Phys. Rev. B* **73**, 104418 (2006).
- ²⁸ N. Büttgen, H.-A. Krug von Nidda, L.E. Svistov, L.A. Prozorova, A. Prokofiev, and W. Assmus, *Phys. Rev. B* **76**, 014440 (2007).
- ²⁹ N. Büttgen, W. Kraetschmer, L.E. Svistov, L.A. Prozorova, and A. Prokofiev, *Phys. Rev. B* **81**, 052403 (2010).
- ³⁰ N. Büttgen, P. Kuhns, A. Prokofiev, A.P. Reyes, and L.E. Svistov, *Phys. Rev. B* **85**, 214421 (2012).
- ³¹ K. Nawa, M. Takigawa, M. Yoshida, and K. Yoshimura, *J. Phys. Soc. Jpn.* **82** 094709 (2013).
- ³² T. Masuda, M. Hagihala, Y. Kondoh, K. Kaneko, and N. Metoki, *J. Phys. Soc. Jpn.* **80**, 113705 (2011).
- ³³ M. Mourigal, M. Enderle, B. Fåk, R.K. Kremer, J.M. Law, A. Schneidewind, A. Hiess, and A. Prokofiev *Phys. Rev. Lett.* **109**, 027203 (2012).
- ³⁴ L.E. Svistov, T. Fujita, H. Yamaguchi, S. Kimura, K. Omura, A. Prokofiev, A.I. Smirnov, Z. Honda, and M. Hagiwara, *JETP Letters* **93**, 21 (2011).
- ³⁵ H.-A. Krug von Nidda, L. E. Svistov, M. V. Eremin, R. M. Eremina, A. Loidl, V. Kataev, A. Validov, A. Prokofiev, and W. Assmus, *Phys. Rev. B* **65**, 134445 (2002).
- ³⁶ F.C. Zhang and T.M. Rice, *Phys. Rev. B* **37**, 3759 (1988).
- ³⁷ H. Tsunetsugu and M.E. Zhitomirsky, private communication (2013).